Microstructure and thermal stability of ultra fine grained Mg-based alloys prepared by high-pressure torsion

J. Čížek [a,*], I. Procházka [a], B. Smola [a], I. Stulíková [a], R. Kužel [a],
Z. Matěj [a], V. Cherkaska [a], R.K. Islamgaliev [b], O. Kulyasova [b]

[a] *Faculty of Mathematics and Physics, Charles University, V Holešovičkách 2, CZ-18000 Praha 8, Czech Republic*
[b] *Institute of Physics of Advanced Materials, Ufa State Aviation Technical University, Ufa 450 000, Russia*

Abstract

The microstructure of ultra fine grained (UFG) Mg and the Mg–9.33 wt.% Gd (Mg10Gd) alloy and its development with temperature were studied in this work. The UFG specimens were prepared by high-pressure torsion (HPT) and investigated using positron lifetime spectroscopy combined with transmission electron microscopy, X-ray diffraction and microhardness measurements. It was found that pure Mg has undergone a substantial recrystallization already in the course of HPT treatment which resulted in a binomial type microstructure. On the other hand, a homogenous UFG structure with a high density of dislocations was formed in HPT-treated Mg10Gd. Investigations of the development of the microstructure with increasing temperature revealed that recovery of dislocations takes place at similar temperatures in both specimens. In the pure Mg it is accompanied by grain growth, while the Mg10Gd exhibits grain growth only at significantly higher temperatures. Moreover, the precipitation sequence in HPT-treated Mg10Gd differs significantly from that in the coarse-grained alloy.
© 2006 Elsevier B.V. All rights reserved.

Keywords: Mg alloys; Severe plastic deformation; Positron annihilation; Defects

1. Introduction

Mg–Gd alloys are promising, novel, light hardenable materials with a high creep resistance, even at elevated temperatures [1]. Despite the favourable strength and thermal stability, a disadvantage of Mg-based alloys consists in a low ductility, insufficient for industrial applications. It is known that ultra fine grained (UFG) metals with a grain size typically of about 100 nm can be produced by high-pressure torsion (HPT) [2]. A number of UFG metals exhibit favourable mechanical properties consisting in a combination of a very high strength and a significant ductility. Hence, it is highly interesting to examine the microstructure and physical properties of UFG Mg-based light alloys. Consequently, microstructure and defect studies of HPT-treated pure Mg and Mg10Gd alloy were performed in the present work. The characterization of lattice defects was undertaken by positron lifetime (PL) spectroscopy, which is a well

developed non-destructive technique with very high sensitivity to open-volume defects such as vacancies, dislocations, etc. [3]. In this work, PL spectroscopy was combined with transmission electron microscopy (TEM), X-ray diffraction (XRD) and microhardness measurements.

2. Experimental details

Specimens of technically pure Mg and Mg–9.33 wt.% Gd (Mg10Gd) alloy were investigated. Results of chemical analysis of the materials studied are shown in Table 1. The Mg10Gd alloy was prepared by squeeze casting using the technically pure Mg. The as-cast material was subjected to a solution annealing at 500 °C for 6 h followed by quenching into water at room temperature. To fabricate a UFG structure, the as-received Mg and the solution treated Mg10Gd alloy were deformed by HPT at room temperature using five rotations under a high pressure of 6 GPa. Details about the HPT procedure can be found in Ref. [2]. The HPT-treated specimens are disk shaped with a diameter of ≈12 mm and a thickness of ≈0.3 mm. The true logarithmic strain $e = 7$ at the outer edge of the specimen can be calculated

* Corresponding author. Tel.: +420 2 2191 2788; fax: +420 2 2191 2765.
E-mail address: jcizek@mbox.troja.mff.cuni.cz (J. Čížek).

Table 1
Results of chemical analysis of the materials studied

Sample	Gd (wt.%)	Mn (wt.%)	Fe (wt.%)	Zn (wt.%)	Al (wt.%)	Si (wt.%)	Cu (wt.%)	Ni (wt.%)	Mg
Mg	–	0.014	0.020	0.0001	0.0077	0.0090	0.0026	0.0004	Balance
Mg10Gd	9.33	0.014	0.020	0.0001	0.0077	0.0090	0.0026	0.0004	Balance

using the equation [2]

$$e = \ln\left(\frac{\upsilon r}{l}\right), \tag{1}$$

which is widely used for HPT-treated materials. The symbol υ denotes the rotation angle in radians, r and l are the radius and thickness of the sample disk, respectively. The strain in a sample increases from zero in the centre to a maximum value at the outer edge. However, at the same time the results of numerous investigations show that after several rotations the deformation often results in a similar refinement of the microstructure in the centre of the sample as well as at the outer edge, see e.g. Ref. [2] and the references wherein. The reason is that the formation of the UFG structure during HPT occurs as an effect of both external and internal stresses. Unfortunately, Eq. (1) is not rigidly bounded with values of the internal stresses. Thus, the true strain according to Eq. (1) is only approximately equal to the real strain in the sample. Because of these difficulties, it is may be more reasonable to consider the number of rotations and not the strain value calculated by the analytical equation.

Some rise of specimen temperature during HPT treatment is expected. Unfortunately, direct measurement of HPT-treated specimen temperature is difficult. To estimate the importance of the temperature rise effect for the development of the UFG structure, we used the results obtained on specimens deformed by equal channel pressing (ECAP). A direct measurement of temperature rise in Al rods during ECAP deformation with a pressing speed of 18 mm s^{-1} performed by Yamaguchi et al. [4] showed that the increase in specimen temperature did not exceed 40 °C. An even lower increase of temperature is expected for a specimen deformed by HPT, because (i) a small size disk shaped specimen placed on a massive steel support is deformed, i.e. the heat evacuation is pretty good and (ii) the deformation rate used in HPT is lower than in ECAP. Thus, we conclude that the temperature rise in HPT-treated specimen is lower than 40 °C.

A fast–fast spectrometer similar to that described in Ref. [5] with a time resolution of 170 ps was used in this work. The decomposition of PL spectra into exponential components was undertaken using a maximum likelihood procedure [6]. Transmission electron microscopy (TEM) was carried out on a JEOL 2000 FX electron microscope operating at 200 kV. X-ray diffraction (XRD) studies were performed using XRD7 and HZG4 (Seifert-FPM) powder diffractometers with Cu Kα radiation. The Vickers microhardness, HV, was measured at a load of 1 N applied for 10 s using a LECO M-400-A hardness tester.

3. Results and discussion

The microstructure of the initial coarse-grained Mg and Mg10Gd (i.e. prior to HPT treatment) has been described in

Ref. [7]. The coarse-grained Mg exhibits a dislocation density of $\rho \approx 5 \times 10^{12}$ m^{-2} and the mean grain size of about 10 μm. The solution treated Mg10Gd alloy is characterized by large coarse grains and a dislocation density below 10^{12} m^{-2} [7].

A bright-field TEM image and an electron diffraction pattern of HPT-treated Mg are shown in Fig. 1. Two different types of regions were observed: (i) "deformed regions" with UFG grains (100–300 nm) and a high density of dislocations and (ii) "recrystallized regions" with substantially larger grains (1–5 μm) and almost free of dislocations. The presence of the "recrystallized regions" indicates an incomplete dynamic recovery of the microstructure during HPT processing. The XRD back-reflection pattern is a superposition of isolated spots and continuous diffraction rings, which testifies the co-existence of the two types of regions. The specimen exhibits a (0 0 0 1) type texture. There was no significant broadening of the XRD profiles. It indicates that the dislocation density should be less than about of 10^{13} m^{-2}. However, a major contribution to the diffraction peaks comes from the "recrystallized regions" so that the "deformed regions" cannot be sufficiently well characterized by XRD. The PL spectrum of HPT-treated Mg consists of the free positron component with lifetime τ_1 and intensity I_1 and a contribution of positrons trapped at defects (lifetime τ_2 and intensity I_2), see Table 2. The intensities are normalized so that $I_1 + I_2 = 100\%$. The lifetime τ_2 of the latter component agrees
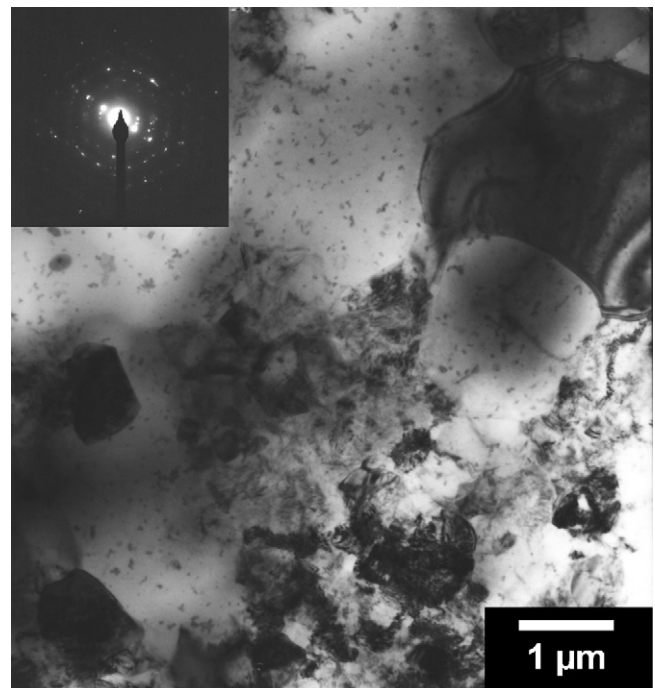

Fig. 1. Bright-field TEM image of HPT-treated Mg.

Table 2
Lifetimes and corresponding relative intensities of the exponential components resolved in PL spectra (except of the source contribution)

Sample	τ_1 (ps)	I_1 (%)	τ_2 (ps)	I_2 (%)
HPT-treated Mg	188(5)	39(1)	257(3)	61(1)
HPT-treated Mg10Gd	180(4)	34(2)	256(3)	66(2)

The errors (one standard deviation) are given in parentheses.

well with that found in a cold rolled Mg for positrons trapped at dislocations [7]. Hence, we can conclude that positrons in HPT-treated Mg are trapped at dislocations inside the "deformed regions". A picture of positron trapping at dislocations proposed firstly by Smedskjaer et al. [8] is nowadays generally accepted. Dislocations are only shallow traps for positrons. Once a positron is trapped at a dislocation, it diffuses quickly along the dislocation line (pipe diffusion) and is finally trapped at a vacancy anchored in the dislocation elastic field or at a jog on the dislocation. Hence, the dislocation line is only a precursor for positron trapping, while the final annihilation site is a vacancy-like defect. That is why positron lifetimes for dislocations are typically only a few picoseconds shorter than those for vacancies, see e.g. Ref. [3]. By the statement "positron trapping at dislocations" used in the paper for shortening we mean the trapping process explained above.

A bright-field TEM image and an electron diffraction pattern for the HPT-treated Mg10Gd alloy are shown in Fig. 2. The image shows a uniform UFG microstructure with a mean grain size of about 100 nm, i.e. no dynamic recovery took place during HPT processing. The electron diffraction pattern shows high-angle missorientation of neighboring grains. A high density of homogeneously distributed dislocations was also observed.
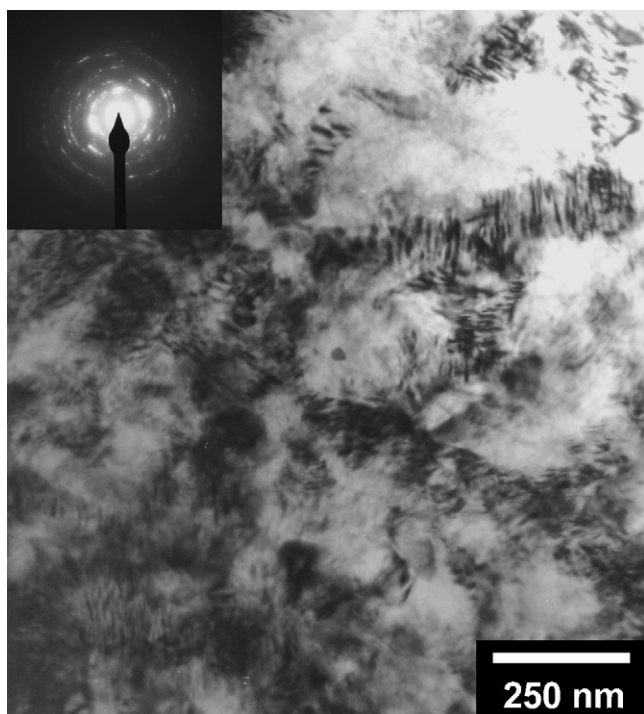

Fig. 2. Bright-field TEM image of HPT-treated Mg10Gd.

A high dislocation density can be deduced also from a significant broadening of the XRD profiles. Less broadening of (0 0 0 1) profiles with respect to other peaks indicates the dominating presence of $\langle a \rangle$ dislocations with the Burgers vector $\boldsymbol{b} = 1/3 \cdot a \cdot \langle 2\,\bar{1}\,\bar{1}\,0 \rangle$. A weak (0 0 0 1) texture was found. The PL spectrum of the HPT-treated Mg10Gd alloy consists of two components, see Table 2. The first component with a lifetime τ_1 arises from the free positrons. The lifetime τ_2 of the second component corresponds well with the lifetime of positrons trapped at Mg-dislocations [7]. Detailed mapping of the specimen by microhardness measurements at various positions revealed out that there is a slight increase in dislocation density from the centre of the specimen towards the outer edge, see Ref. [7] for details. Positron annihilation measurements performed at various distances from the centre of HPT-treated specimens confirmed this conclusion. The observed increase of dislocation density can be expected because of the increasing strain from the specimen centre towards the edges.

Vacancy clusters (called "microvoids" or sometimes also "nanovoids") were detected in a number of fcc and bcc UFG metals, like Cu, Fe, Ni, Al, see e.g. Refs. [9–11]. Similar defects have been found also in nanocrystalline Cu and Fe [12,13]. On the contrary no component which could be attributed to microvoids was detected in the PL spectra of HPT-treated Mg and Mg10Gd alloy, see Table 2. It indicates that the concentration of microvoids in the studied specimens is very low and does not exceed 10^{-6} at.$^{-1}$. It is assumed that microvoids in UFG metals are formed by clustering of vacancies introduced during severe plastic deformation. Dislocations in fcc and bcc metals are situated mostly in layers along grain boundaries, while the grain interiors are virtually free of dislocations [14]. On the other hand, Fig. 2 shows that HPT-treated Mg10Gd alloy exhibits uniform distribution of dislocations throughout the whole specimen. Similarly, a high density of equally spaced dislocations is observed in the "deformed regions" in HPT-treated Mg, see Fig. 1. Closely spaced dislocations facilitate diffusion of vacancies to sinks at grain boundaries by pipe diffusion along the dislocation line, while agglomeration of vacancies, and thereby also formation of microvoids, is suppressed. That is why we do not detect microvoids in HPT-treated Mg and Mg10Gd alloy.

It should be noted that the mean positron penetration depth in Mg is 152 μm [3]. Thus, PL spectroscopy probes bulk properties of the samples studied, while sensitivity to surface features is rather low. For example, only 0.7% of positrons annihilates in a depth smaller than 1 μm from the surface. Based on our PL measurements we concluded that the concentration of microvoids in the bulk is negligible ($<10^{-6}$ at.$^{-1}$). However, one cannot exclude a certain concentration of microvoids and/or voids in the surface layer, which are not detected by PL measurements.

After characterization of the as-deformed microstructure, the specimens were subjected to isochronal annealing in order to study the development of microstructure with increasing temperature and the recovery of defects. The PL spectra of HPT-treated Mg and Mg10Gd specimens consisted of the two components with lifetimes τ_1 (free positrons) and τ_2 (positrons trapped at
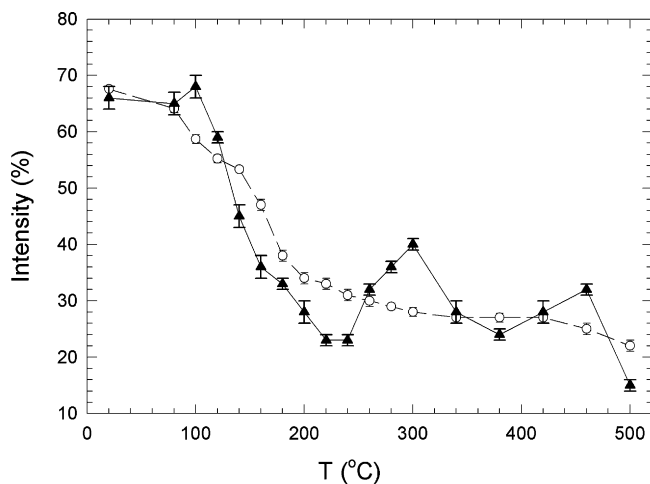
Fig. 3. Temperature dependence of the relative intensity I_2 of positrons trapped at dislocations for HPT-treated Mg (open circles) and HPT-treated Mg10Gd (full triangles).

dislocations) at all the annealing temperatures. The lifetime τ_2 did not change with annealing temperature (except for some statistical fluctuations) indicating that the nature of positron traps remains unchanged. Therefore, in order to decrease statistical fluctuations of the fitted parameters, the lifetime τ_2 was fixed at 256 ps in the final analysis of PL spectra. The relative intensity I_2 of the dislocation component for HPT-treated Mg and Mg10Gd is plotted in Fig. 3 as a function of the annealing temperature. Fig. 4 shows the temperature dependence of the microhardness, HV, for the both specimens. The HV of Mg10Gd increases from the specimen centre towards the outer edge. Thus, the minimum and maximum HV values corresponding to the centre and the outer edge of the specimen are shown in Fig. 4 for each temperature. It is obvious in Fig. 3 that HPT-treated Mg shows a dramatic decrease in I_2 from room temperature to 200 °C. The regions with the UFG structure and a high density of dislocations are gradually replaced by dislocation-free recrystallized grains. The typical size of the recrystallized grains is about 5 μm. As mentioned above, the recrystallization process occurs already at room temperature during the HPT processing. Although the HPT-treated Mg has already undergone a substantial recrystallization in the course of HPT treatment, the TEM observations clearly showed that it still contains a significant volume fraction of "deformed regions" with a high density of dislocations. The replacement of the "deformed regions" by the dislocation-free recrystallized grains leads to a softening as seen from the strong decrease in microhardness, see Fig. 4. The largest drop in HV occurs in the temperature range (20–150 °C). Eventually, at ≈200 °C the specimen exhibits a completely recrystallized structure with a low dislocation density $\rho \approx 1 \times 10^{12}$ m^{-2} and the mean grain size ≈5 μm, see Fig. 5. The recrystallized structure remains essentially the same after annealing to higher temperatures.

The decomposition of supersaturated solid solutions (sss) and the precipitation effects in solution treated (i.e. coarse-grained) Mg10Gd alloy were studied in details elsewhere [1,15]. The decomposition takes place in the sequence: sss → β″
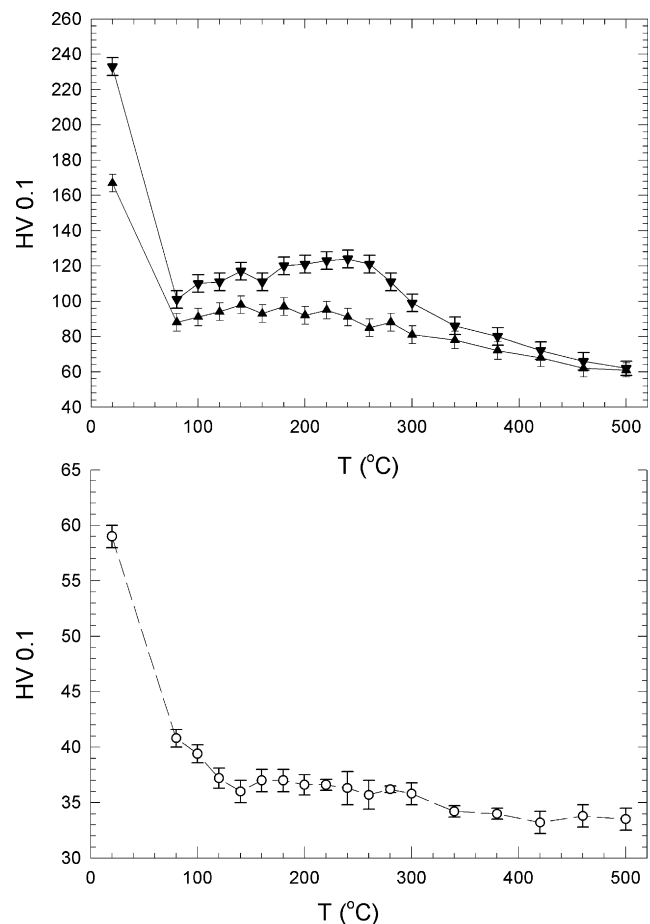

Fig. 4. Temperature dependence of microhardness, HV. Upper diagram—HPT-treated Mg10Gd (full triangles). The triangles oriented upwards show minimum HV corresponding to the centre of the sample, the triangles oriented downwards show maximum HV corresponding to the edge. Lower diagram—HPT-treated Mg (open circles).

(D019) → β′ (c-base centered orthorhombic) → β (Mg$_5$Gd, cubic). The β″ and β′ are metastable phases and β is the high temperature stable phase.

It was found that the precipitation effects in HPT-treated Mg10Gd differ significantly from those in the corresponding coarse-grained material. It is clear from Fig. 3 that a radical decrease in I_2 takes place in the temperature interval (100–220 °C) in HPT-treated Mg10Gd. It indicates a significant recovery of dislocations in this temperature range. A slight local increase in I_2 at 100 °C is likely, due to the formation of the β″ phase as confirmed by coincidence Doppler broadening [16]. However, the β″ phase particles are very fine (10 nm in diameter or less) and were thus not observed by TEM. It should be noted, that the high dislocation density makes TEM observation of fine precipitates very difficult. It can be seen in Fig. 4 that HV for HPT-treated Mg10Gd falls abruptly after anneal at 80 °C, i.e. it precedes the decrease in I_2, see Fig. 3. It indicates that there is a remarkable softening which seems to occur prior to the decrease in dislocation density. It could be connected with some rearrangement of dislocations without significant change of the net dislocation density or by relaxation of internal stresses introduced in the specimen by severe plastic deforma-
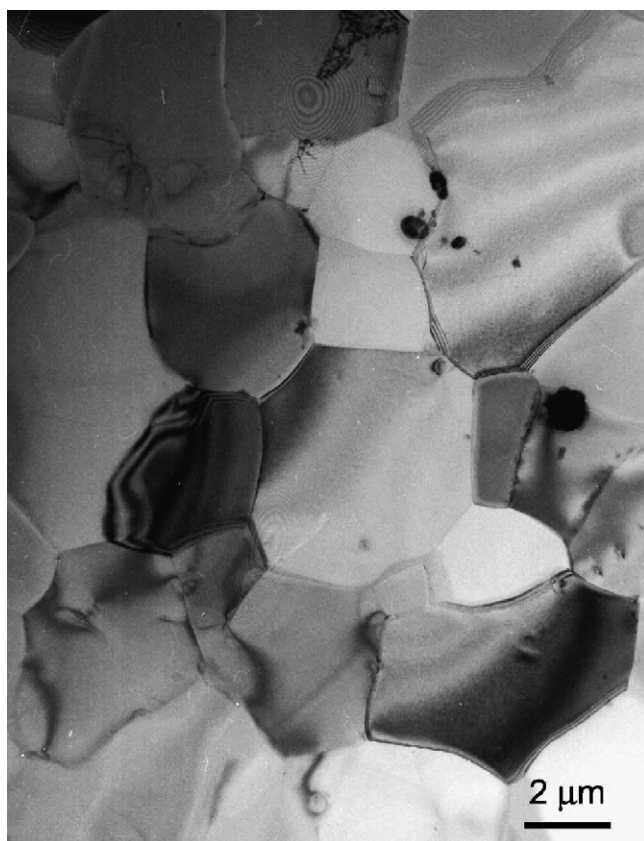
Fig. 5. Bright-field TEM image of HPT-treated Mg annealed up to 200 °C.

tion. Another alternative is that nucleation of the β″ phase starts already at 80 °C. Positron trapping at new defects introduced by the nucleation of the β″ phase prevents the decrease of I_2 even when the dislocation density decreases. Contrary to HPT-treated Mg, in the case of HPT-treated Mg10Gd the initial drop in HV is reversed at 100 °C by a slight increase caused by formation of fine precipitates of the β″ phase which cause a weak precipitation hardening. At the same time recovery of dislocations continues which is confirmed by a strong decrease in I_2. Thus, in the temperature range 100–220 °C two competitive processes take place in the HPT-treated Mg10Gd specimen: (i) precipitation hardening and (ii) softening caused by recovery of dislocations. At higher temperatures the metastable β″ phase dissolves and particles of the stable β phase are formed. The β phase precipitates were identified by TEM in the specimen annealed up to 260 °C. Finely dispersed incoherent particles of the β phase cause higher hardening which is reflected by a local maximum of HV at 250 °C. Further growth of the β phase precipitates leads again to a decrease of HV above 250 °C

A bright-field TEM image of HPT-treated Mg10Gd annealed at 260 °C is shown in Fig. 6. A significant decrease in the dislocation density in the grains can be clearly seen. However, the grain size does not increase and remains at about 100 nm. Thus, contrary to HPT-treated Mg, the recovery of dislocations in HPT-treated Mg10Gd is not accompanied by grain growth. The TEM observations have shown that the mean grain size remains at about 100 nm up to ≈300 °C demonstrating very good thermal stability of the UFG structure in HPT-treated Mg10Gd. A local
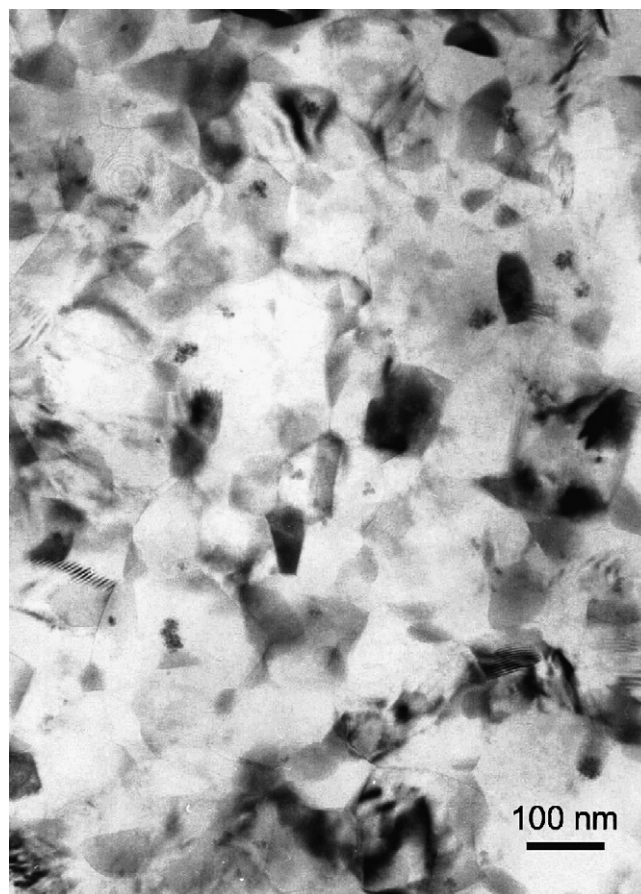

Fig. 6. Bright-field TEM image of HPT-treated Mg10Gd annealed up to 260 °C.

maximum of I_2 at 300 °C is due to the precipitation of the equilibrium β phase. It is in concordance with the HV curve. Positrons are trapped at the misfit defects between the incoherent β phase particles and the matrix. This results in a local increase in I_2. Coarsening of the β phase particles causes a subsequent decrease in I_2, see Fig. 3. Above 450 °C, the β phase particles dissolve and the solid solution is restored.

From our investigations we can conclude that the precipitation sequence in HPT-treated Mg10Gd differs significantly from that known in corresponding coarse-grained material. Contrary to the coarse-grained alloy, precipitation of the metastable β′ phase is absent in HPT-treated Mg10Gd and the stable β phase is formed at significantly lower temperatures.

4. Summary

The microstructure of HPT-treated Mg and Mg10Gd and its development with temperature were characterized. An incomplete dynamic recovery took place during HPT processing of the Mg specimen. It results in a binomial kind of structure. The HPT-treated Mg10Gd exhibits a homogeneous UFG microstructure with a high density of uniformly distributed dislocations and a grain size around 100 nm. Recovery of dislocations occurs already at room temperature in HPT-treated Mg and is accompanied by recrystallization. On the other hand, Mg10Gd exhibits a dramatic decrease in dislocation density in the temperature

range (100–220 °C) but no grain growth takes place. The mean grain size in HPT-treated Mg10Gd remains at about 100 nm up to ≈300 °C. There are significant differences in the precipitation sequence in HPT-treated Mg10Gd and corresponding coarse-grained alloy: the formation of the metastable β′ phase does not occur and the precipitation of the stable β phase is shifted to lower temperatures.

Acknowledgements

References

[1] P. Vostrý, B. Smola, I. Stulíková, F. von Buch, B.L. Mordike, Phys. Status Solidi (a) 175 (1999) 491–500.

[2] R.Z. Valiev, R.K. Islamgaliev, I.V. Alexandrov, Prog. Mater. Sci. 45 (2000) 103–189.

[3] P. Hautojärvi, C. Corbel, in: A. Dupasquier, A.P. Mills (Eds.), Proceedings of the International School of Physics "Enrico Fermi", Course CXXV, IOS Press, Varenna, 1995, pp. 491–562.

[4] D. Yamaguchi, Z. Horita, M. Nemoto, T.G. Langdon, Scripta Mater. 41 (1999) 791–796.

[5] F. Bečvář, J. Čížek, L. Lešt'ak, I. Novotný, I. Procházka, F. Šebesta, Nucl. Instrum. Methods A 443 (2000) 557–577.

[6] I. Procházka, I. Novotný, F. Bečvář, Mater. Sci. Forum 225–257 (1997) 772–775.

[7] J. Čížek, I. Procházka, B. Smola, I. Stulíková, R. Kužel, Z. Matěj, V. Cherkaska, R.K. Islamgaliev, O. Kulyasova, Mater. Sci. Forum 482 (2005) 183–185.

[8] L.C. Smedskjaer, M. Manninen, M.J. Fluss, J. Phys. F: Met. Phys. 10 (1980) 2237–2249.

[9] R. Würschum, W. Greiner, R.Z. Valiev, M. Rapp, W. Sigle, O. Schneeweiss, H.-E. Schaefer, Scripta Metall. Mater. 25 (1991) 2451–2456.

[10] J. Čížek, I. Procházka, M. Cieslar, R. Kužel, J. Kuriplach, F. Chmelík, I. Stulíková, F. Bečvář, O. Melikhova, R.K. Islamgaliev, Phys. Rev. B 65 (2002) 094106.

[11] J. Čížek, I. Procházka, M. Cieslar, I. Stulíková, F. Chmelík, R.K. Islamgaliev, Phys. Status Solidi (a) 191 (2002) 391–408.

[12] R. Würschum, M. Scheytt, H.-E. Schaefer, Phys. Status Solidi (a) 102 (1987) 119–126.

[13] H.-E. Schaefer, R. Würschum, R. Birringer, H. Gleiter, Phys. Rev. B 38 (1988) 9545–9554.

[14] R.K. Islamgaliev, F. Chmelík, R. Kužel, Mater. Sci. Eng. A 237 (1997) 43–51.

[15] J. Čížek, I. Procházka, B. Smola, I. Stulíková, R. Kužel, Z. Matěj, V. Cherkaska, Phys. Status Solidi (a) 203 (2006) 466–477.

[16] J. Čížek, I. Procházka, B. Smola, I. Stulíková, R. Kužel, Z. Matěj, V. Cherkaska, R.K. Islamgaliev, O. Kulyasova, Acta Phys. Polym. A 107 (2005) 738–744.